remote sensing

MDPI

Technical Note

Effects of the Architectural Layout of the Sanctuary of Pachacamac (2nd–16th Century CE, Peru) on the Exposure to Rain, Wind, and Solar Radiation from the Morphometric Analysis of Digital Surface Models

Luigi Magnini [1], Denise Pozzi-Escot [2], Janet Oshiro [2], Rommel Angeles [2], Maria Ilaria Panaccione Apa [3] and Guido Ventura [3,*]

[1] Dipartimento di Studi Umanistici, Università Ca' Foscari di Venezia, 30100 Venezia, Italy; luigi.magnini@unive.it
[2] Museo Pachacamac, Ministerio de Cultura, Distrito de Lurín, 15800 Lima, Peru; dpozzi@cultura.gob.pe (D.P.-E.); joshiro@cultura.gob.pe (J.O.); rangeles@cultura.gob.pe (R.A.)
[3] Istituto Nazionale di Geofisica e Vulcanologia, 00143 Rome, Italy; mariailaria.pannaccioneapa@ingv.it
* Correspondence: guido.ventura@ingv.it; Tel.: +39-06-5186-0221

Abstract: Natural events (floods, earthquakes, landslides, etc.) may significantly damage archaeological sites, and therefore reducing their exposure to such events represents a priority for protective and conservation activities. The archaeological Sanctuary of Pachacamac (SP; 2nd–16th century CE; Peru) covers an area of 465 hectares and includes roads, enclosures, huacas with ramps, temples, and palaces located along the central coast of Peru. This area is affected by heavy rain and winds related to the El Niño–Southern Oscillation and to intense solar radiation. We use a 30 cm resolution Digital Surface Model obtained from orthophotogrammetric data and perform a morphometric analysis using geomorphological, hydrological, and climatic quantitative parameters. Our aim is to identify the zones exposed to water flow or stagnation during rainfall, as well as the exposure to winds and solar radiation. The calculated parameters are subsequently processed with an object-based image analysis approach to identify areas with higher climate exposure. We show that the SP architectural layout controls the exposure to water stagnation or flow in the form of rainfall, whereas exposure to wind and solar radiation mainly depends on the topography of an area (e.g., the presence of hills and plains). The methodological approach proposed here may be applied and extended to other archaeological sites.

Keywords: archaeological heritage; morphometry; UAV remote sensing; climate; natural hazard exposure

Citation: Magnini, L.; Pozzi-Escot, D.; Oshiro, J.; Angeles, R.; Apa, M.I.P.; Ventura, G. Effects of the Architectural Layout of the Sanctuary of Pachacamac (2nd-16th Century CE, Peru) on the Exposure to Rain, Wind, and Solar Radiation from the Morphometric Analysis of Digital Surface Models. *Remote Sens.* **2024**, *16*, 1848. https://doi.org/10.3390/rs16111848

Academic Editor: Dimitrios D. Alexakis

Received: 1 May 2024
Revised: 20 May 2024
Accepted: 20 May 2024
Published: 22 May 2024

1. Introduction

The management and conservation of archaeological sites and cultural heritage allow us to preserve testimonies of human activities, reconstruct the past, and better recognize the interactions between human societies and the environment [1,2]. The UN's 2030 Agenda for Sustainable Development includes, among various objectives, the intention to "strengthen efforts to protect and safeguard the world's cultural and natural heritage" [3]. Another reason for the importance of archaeological heritage is that it may act as a flywheel of social and economic development. Many archaeological sites are, however, exposed to anthropic activities and natural hazardous events. The latter include earthquakes, erosion processes, gravity instability, floods, heavy rain and wind events, and anomalous increases in temperature as a result of climate change [4]. Therefore, identifying natural events that are potentially able to deteriorate or, in some cases, destroy

archaeological sites, and the recognition of the areas exposed to these events, is a prerequisite of fundamental importance when it comes to protecting the testimonies of the past [5]. In this framework, the actions aimed to reduce the effects of hazardous natural events can be implemented if an evaluation of the spatial distribution of the physical processes associated with such potentially damaging events is available [6–8]. The identification of the areas of archaeological sites with exposure to the natural hazards summarized above requires a multidisciplinary integration of quantitative spatial and morphological/physical data. Remote sensing data from satellite platforms, aerophotogrammetric surveys, and terrestrial and airborne laser scanners provide high-resolution measurements which may be used to reconstruct archaeological structures and quantify their degree of preservation [9–18]. These data, when combined with information from geomorphological and climate/meteorological data, can be used to determine archaeological sites' degree of exposure to hazards [19–25].

The archaeological site of the Sanctuary of Pachacamac (hereafter SP, 2nd to 16th centuries CE) is located on the central coast of Peru (Figures 1 and 2).

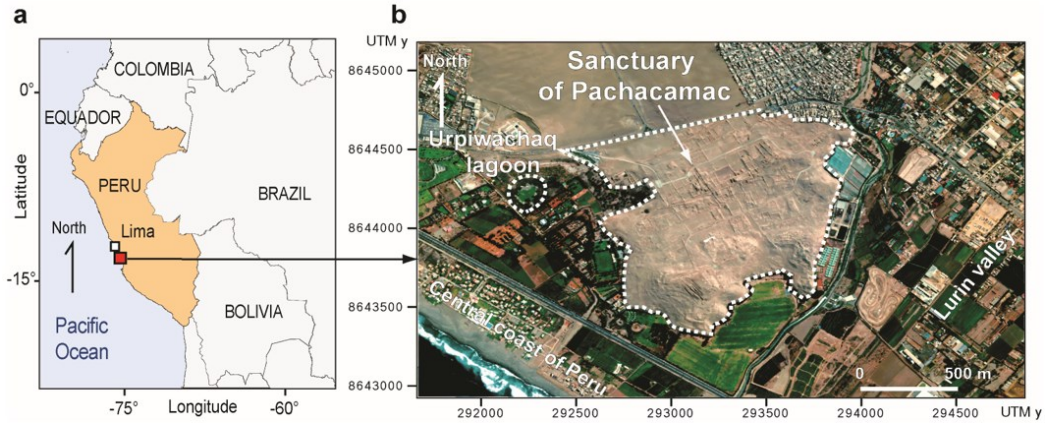

Figure 1. (**a**) Location map of the Sanctuary of Pachacamac. (**b**) Satellite image of the archaeological area (GoogleEarthPro, Image 2022@ Maxar Technologies).

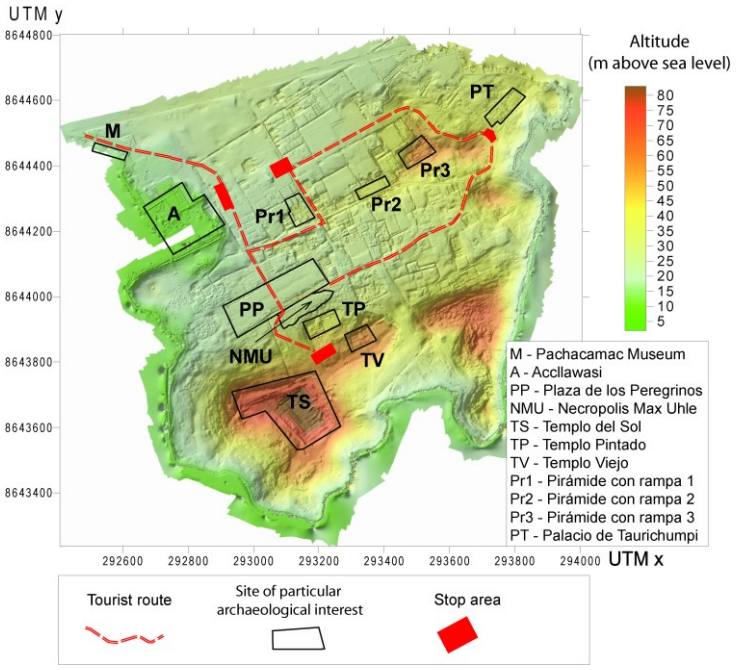

Figure 2. Shaded relief and altitude of the Sanctuary of Pachacamac according to a Digital Surface Model. The location of the main sites of archaeological interest and the tourist route are also reported.

SP covers an area of 465 hectares, and it is exposed to the events related to the El Niño–Southern Oscillation [26]. Heavy rain, intense winds, and hot airflow in the semi-arid region of the Peruvian coast increased with the El Niño frequency over the last 3200–2800 years and were responsible for the abandonment of the coastal settlements in historical and prehistoric times [27]. SP was affected in around 600 CE by rain and flooding related to the 6th century El Niño event [28,29]. More recently, the SP buildings were affected by heavy rain until the 20th century CE, with severe damages resulting from the 1925–1926 El Niño event. Therefore, SP has been identified as a potential hazard due to the El Niño meteorological and climatic phenomena. The intensity of the El Niño rainfall and wind in Peru is expected to increase in the next few years due to climate change [30]. Here, we use orthophotogrammetric data collected on the SP archaeological site to reconstruct its present-day 3D structure and perform a morphometric study with the aim of identifying (a) the areas subjected to water flow or stagnation during rainfall, (b) the exposure of the building to the wind and sun in a semi-arid region. We use this approach because the results from other types of analyses, such as the impact of a set of modeled rain events, could provide unrealistic results due to the lack of reliable and long/medium term data and the impossibility to forecast the magnitude of the El Niño events over years [31]. Therefore, an approach based on the probabilistic or deterministic, e.g., scenario-based evaluation of the intensity of natural phenomena and their future changes, which represents the "standard procedure" for the assessment of hazard of a territory [32,33], cannot be reasonably applied to the SP area. To perform our analysis of SP, selected morphometric parameters indicative of the above-described types of exposure are extracted from a Digital Surface Model (DSM). These parameters are subsequently processed together with an Object-based Image Analysis (OBIA) approach to identify areas with a higher probability of climate exposure and to obtain more comparable and reproducible results [34–36]. The methodological workflow used here is transferable to other sites at different locations and may be useful for assessing the vulnerability of archaeological sites and planning actions designed to protect our cultural heritage.

2. Sanctuary of Pachacamac

2.1. Terrain Morphology and Main Structures

The SP monumental archaeological complex is located on the central coast of Peru, 30 km south of Lima (Figure 1), and it is a part of the Inca Road network "Qhapaq Ñan" [37], which integrated Cuzco, the capital of the Inca Empire, with the entire Inca territory through an organized system of roads and administrative centers [38,39]. In 2014, UNESCO declared "Qhapaq Ñan" a World Cultural Heritage Site, including the Xauxa–Pachacamac section, which connects the Pacific coast with the Andes and the capital of the Inca Empire. SP occupies a relatively flat area with three major hills (Figures 1 and 2).

Two hills are up to 60 m high, ENE-WSW-elongated, and delimit the southern sector of SP. The third hill is 30 m high and is in the northeastern sector of the site (Figure 2). SP is made up of a set of monumental structures dating from the 2nd to 1533 CE [40–42] (Table 1). These structures include large buildings such as Templo Viejo (3rd to 9th centuries CE), huacas (stepped structures) with access ramps (12th to 16th centuries CE), Templo Pintado (8th to 16th centuries CE), Acllawasi, and Templo del Sol (15th-16th centuries CE) (Figure 2). Templo del Sol is located on the top of the highest hill of SP, at the southwestern corner of the archaeological area. Streets, squares, cemeteries, and various enclosures built mostly with adobes and edged stone are also present in the flat area of SP (Figure 2). Notably, the longer perimetral walls of the major buildings (Templo Viejo, Templo Pintado, Templo del Sol), as well as those delimiting the main enclosures (e.g., Plaza del los Peregrinos) and huacas (e.g., Huacas with ramps 1, 2, and 3 in Figure 2), follow a main WNW-ESE strike. This is an architectural element that characterizes the whole SP site.

Table 1. Chronology and main architectural structures of the Sanctuary of Pachacamac. Data from [42].

Dating	Period	Culture (Coast of Peru)	Architecture
1470 AD	Horizonte Tardío (Late Horizon Period)	Inca	Acllawasi (House of Sacred Weavers) Templo Del Sol (Temple of the Sun) Taurichumpi (Governor Palace) Building 47 Plaza de los Peregrinos (Pilgrims Square) House Of Quipus
1100 AD	Intermedio Tardío (Late Intermediate Period)	Ychsma Chancay Casma	Huacas with ramps
600 AD	Horizonte Medio (Middle Horizon Period)	Teatino Pachacamac Nievería	Templo Pintado (Painted Temple) Uhle Necropolis (Cementerio Uhle)
0 AD	Intermedio Temprano (Early Intermediate Period)	Recuay Lima Miramar	Adobites Set (Little Mud Bricks) Urpiwachaq Temple Templo Viejo (Old Temple)

2.2. History

The development of the SP area in historical times was relatively complex. Starting from the Early Intermediate Period (Table 1), the Lima culture began to construct a ceremonial nucleus, converting Pachacamac into an important cultic and administrative center [43], particularly in the wake of the erection of Urpimachac Temple, Templo Viejo (TV in Figure 2), which is made from "adobitos" (a mix of straw and sand–silt–clay bricks) with a central courtyard and two levels of platforms around a large central patio [44,45] and remained active until 9th century AD. In the Middle Horizon period (Table 1), Wari occupation is well documented by a vast necropolis excavated by Max Uhle in 1896 [46], known as "Cementerio Uhle", i.e., Necropolis Max Uhule (NMU in Figure 2) and has been subject to immense looting over time. In the Late Intermediate period (Table 1), Pachacamac was under the lordship of Ychsma, who spread a model of huacas, of which three are still well preserved (Hr1; Hr2; Hr3 in Figure 2) [42], and the upper level of Templo Pintado (TP in Figure 2). The foundation of TP is attributed to the Lima culture in the Early Intermediate period. TP is dedicated to the god Pachacamac [47]. In the Late Horizon period (Table 1), Pachacamac belonged to Chinchaysuyu under the Inca domination [48,49], which added new important architectures such as the House of Qipus, Building 47, Plaza de los Peregrinos (PP in Figure 2), and Accllawasi (A in Figure 2). The latter was reconstructed in the 1940s by Julio C. Tello [50,51]. Taurichumpi Palace (Governor Palace) (PT in Figure 2) was superimposed on a previous structure with a ramp, and the same was true of Templo del Sol, also known as Punchau Cancha (TS in Figure 2). TS was also built on the site of a previous temple and represents the most impressive temple built by Incas along the Peruvian coastline. It is elevated on a trapezoidal plan and made up of six platforms and features large ceremonial niches on its western front. Remnants of red and orange paint remain visible on its walls. The long-lived Pachacamac period ended in 1533 CE.

2.3. Environmental Conditions

There is currently insufficient information on the environmental conditions of SP, and the little available information comes from studies carried out on the Urpiwachaq lagoon, which is located to the west of SP between the archaeological site and the coastline of Peru [52,53]. This aquatic ecosystem is relevant to the formation and growth of SP [54]

because of its abundant agricultural and faunal resources [55]. Winsborough and colleagues [29] and Jacay and Oshiro [52] identified three possible tsunami events in the stratigraphy of Urpiwachaq, which probably occurred during the Early Horizon period (Table 1) and caused significant damage and deposition of marine sediments [29,54]. Furthermore, severe drought periods, which also characterize the present-day semi-arid coast of Peru, and heavy, timely-concentrated rain events due to El Niño have been recorded, although without chronological constraints [52]. As previously reported, SP was damaged in around 600 CE by the rain related to the 6th century El Niño event [28,29] and by other similar events that occurred up to the 20th century CE [27]. The last recorded damage resulted from the 1925–1926 El Niño event.

2.4. Damages

Throughout several centuries, ASP was affected by various damages, which were mainly related to heavy rain associated with El Niño/La Niña events, but in some cases were also the result of earthquakes. The walls of the enclosures located in the central–southern area of SP and the architectural structures located on the three hills have deteriorated as a result of such events. The structural collapse of walls is mostly linked to seismic activity and alluvial infiltration, which produced degradation due to site abandonment and lack of maintenance. These factors, along with the effects of wind and elevated temperature due to solar irradiation on painting, affect various elements of construction, such as adobe, mortar, and stones [56]. The weak consistency of the adobes, the building technique used, and the location of SP in a zone with clay and silty rocks covered by a blanket of sand, have favored gravity instability and erosion phenomena, leading to the removal of material by water and wind. The Pachacamac Museum, which was inaugurated in 2016 and has had a Management Plan since 2014, has implemented various measures to reduce the damage of walls in a critical situation or at risk of collapse. The conservation work is ongoing. Also, the Pachacamac Museum has the objectives of conserving and digitalizing the SP structures with the production of high-resolution orthophotos and DSMs. The tourist route and the associated stopping areas within the SP area exclude visitors from the construction areas that would expose them to potential collapses, such as the Templo del Sol (Figure 2). However, these tourist infrastructures do not consider the potential effects of heavy rain, intense winds, and sun exposure.

3. Materials and Methods

3.1. Orthophotogrammetric Survey and DSM

The orthophotogrammetric survey of SP was carried out between 2019 and 2020 as part of the digital capture activities carried out by the Pachacamac Museum. Here, we summarize the acquisition procedure and methods. Details may be found in the work of Chipana and colleagues [57]. The survey flights were carried out at heights between 35 m and 50 m with a Phantom 4 pro v.2.0 drone equipped with a 20 Mpx camera and GPS. The flights followed a grid pattern using targets on the ground at the edges and center of the flight polygons. On average, the spatial density of the targets was 3 targets/100 m^2. The targets functioned as control points that allowed the survey geo-referencing to occur. The control points were measured with a TOPCON Hiper H differential GPS. Aerial photographs were taken during the flights, and oblique photographs were taken manually. The spatial density of the photographs was, on average, 1500–2000 photographs/5000 m^2. However, because the data were acquired at different times and with different resolutions (from 5 cm to 30 cm/pixel), we homogenize the whole dataset using Agisoft Metashape V. 1.5.3 (https://www.agisoft.com/ (accessed on 20 February 2024)), and a Digital Surface Model (DSM) of SP was created. The DSM has a resolution of 30 cm/px with estimated errors of 3 cm on x and y and 2 cm on z. Figure 2 shows the DSM obtained by the orthophotogrammetric survey and Figure 3a shows the derived slope map.

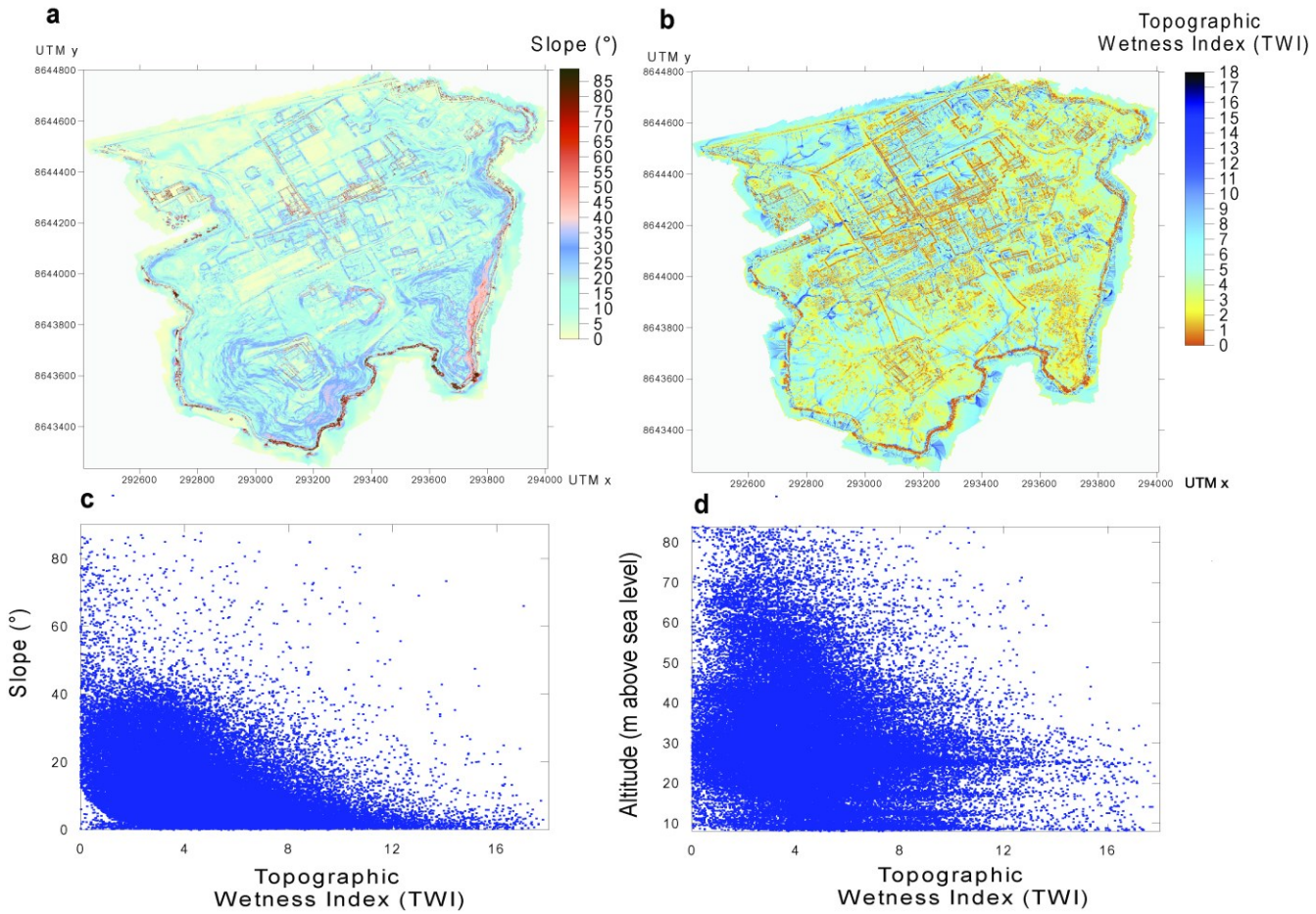

Figure 3. (**a**): Slope map of the Sanctuary of Pachacamac derived from the DSM; (**b**): topographic wetness index (TWI) map derived from the DSM; (**c**): TWI vs. slope values plot; (**d**): TWI vs. altitude plot.

3.2. Morphometric Analysis and Parameters

The aim of the morphometric analysis based on the acquired DSM is to identify the areas of SP potentially exposed to the following events:

1. Water flow or stagnation during the rainfalls related to forthcoming El Niño episodes with the caveat that the intensity of heavy rainfall episodes is very difficult to predict [58].
2. Wind coming off the sea level [59] given that TS is located 1 km northwest of the central coast of Peru.
3. Direct incoming solar radiation as experienced in the semi-arid climatic conditions of the central coastal area of Peru [60].

We use the topographic wetness index (TWI) to identify the areas where the water may flow and accumulate during rain events [19]. TWI is a dimensionless parameter that is extensively used in the hydrological analysis of landforms because it defines the balance of the catchment water supply and local drainage, providing information on the potential runoff generation [61]. The determination of TWI requires two parameters: the local upslope area draining through a certain point per unit contour length A, and the local slope S in radians. The analytical expression is $TWI = \ln[(A)/\tan(S)]$. We map TWI by applying this formula to the DSM of SP. The obtained distribution of the calculated TWI values is shown in Figure 3b. The first step in determining the areas subject to water stagnation alone is the identification of closed depressions. From a morphological point of view, a closed depression may be defined as an area surrounded by higher ground in all directions [62]. We observe two types of depressions: areas bounded by morphological or

artificial walls and holes related to archaeological excavations, e.g., the Uhle Necropolis). Typically, the areas delimited by walls have a rectangular shape, whereas those resulting from excavations are subcircular. With the aim of mapping the closed depression and estimating their depth, we apply the algorithm proposed by Wang and Liu [63]. The method directly computes a spill elevation value with a least-cost search algorithm, which enables the progressive build of the optimal flow paths and propagates spill elevation values from outlets to interior grid cells. This algorithm has been validated in highly irregular karst terrains by Pardo-Igúzquiza and Dowd [62]. These calculations were performed using the open-source software System for Automated Geoscientific Analyses version 9.01 (https://saga-gis.sourceforge.io/en/index.html (accessed on 2 January 2024)). The results obtained at SP are reported in Figure 4a.

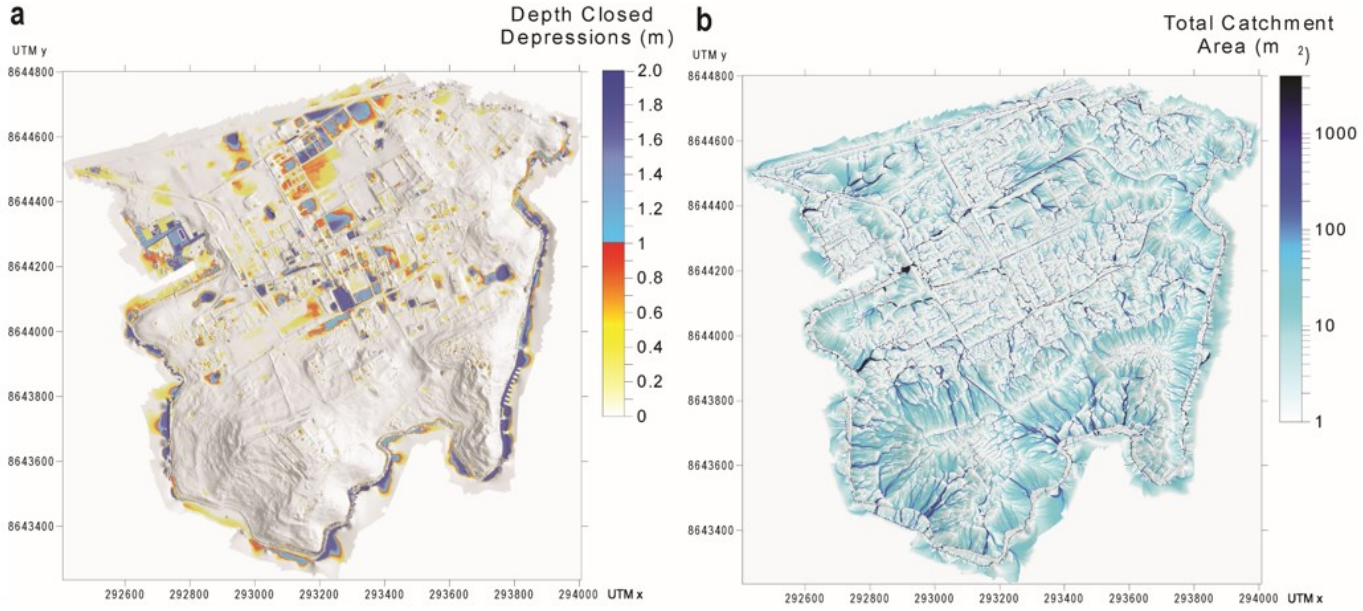

Figure 4. (**a**): Depth of the closed depressions identified from the analysis of the DSM; (**b**): area distribution of the total catchment area derived from the analysis of the DSM.

We determine the total catchment area (TCA) to identify the areas where the water flows and concentrates into streams. The TCA measures the extent of the downslope surface flow pathway. To determine the TCA, we apply the algorithm created by Quinn and colleagues [64], as implemented in the work of Conrad et al. [65], to the DSM. The algorithm allows the accumulated upslope area for any one cell to be distributed amongst all downslope directions. The directions are split into cardinal and diagonal directions with area being able to contribute downhill in up to eight flow directions. The results of the TCA for Pachacamac are reported in Figure 4b.

To measure the exposure of TS to the wind, we adopt a value of N165° as the wind direction, this being the value of the prevailing yearly direction along the central coast of Peru [59]. We determine the extent and degree of upwind or downwind exposure in the DSM by calculating the Wind Effect Index (WEI), which is a dimensionless index. Values of WEI < 1 indicate the areas shielded from the wind, whereas values > 1 indicate areas exposed to wind. In order to calculate the WFI, we use the method described by Boehner and Antonic [66]. The Wind Effect Index is the product of the windward and leeward indexes. These indexes are calculated considering the horizontal distances in windward and leeward directions and the corresponding vertical distances compared with the considered raster cell. The required input parameters are the prevailing wind direction and the digital topography of the study area. The results obtained at SP are reported in Figure 5.

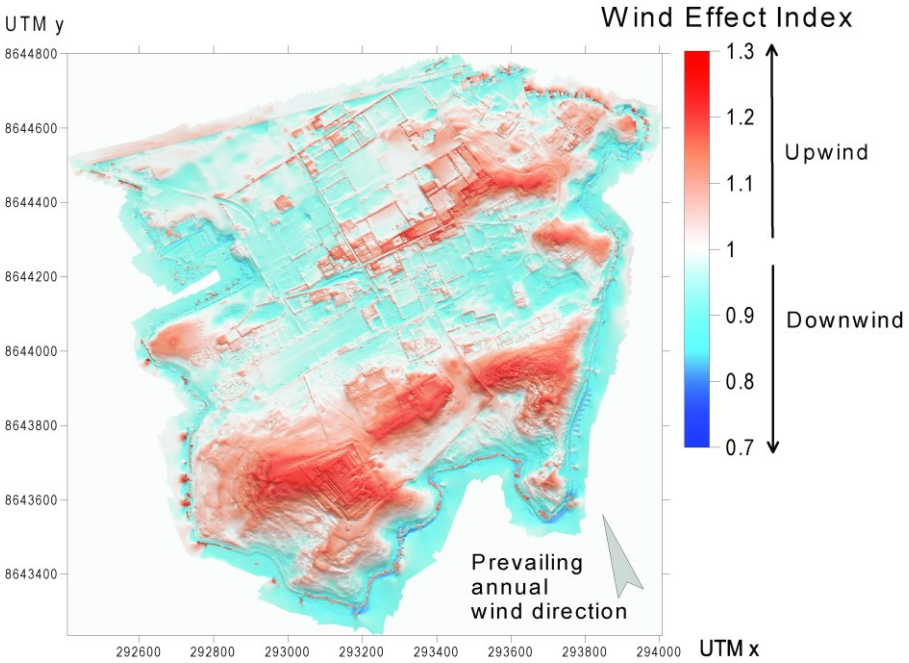

Figure 5. Spatial distribution of the annual exposure to the wind at the Sanctuary of Pachacamac, expressed as the Wind Effect Index.

We use the DSM to map the solar radiation (SR) (Fu and Rich, 1999, 2000, 2002) and the sky view factor (SVF) [67] at SP according to an area-based model, which provides the SR values by integrating the surface orientation and shadow effects on DSMs. SR can be categorized as direct, diffuse, and reflected, with the direct radiation as the main component of the total irradiance. Diffuse radiation is the second component, while reflected radiation is very small and may be disregarded [68]. SVF is a measure of the portion of the sky that is visible from each point of the DSM and provides a non-dimensional parameter between 0 (obscured view) and 1 (completely unobscured view) [69]. SVF also provides an indirect estimate of the diffuse solar radiation [67]. The spatial distribution of SR and SVF at SP is reported in Figure 6.

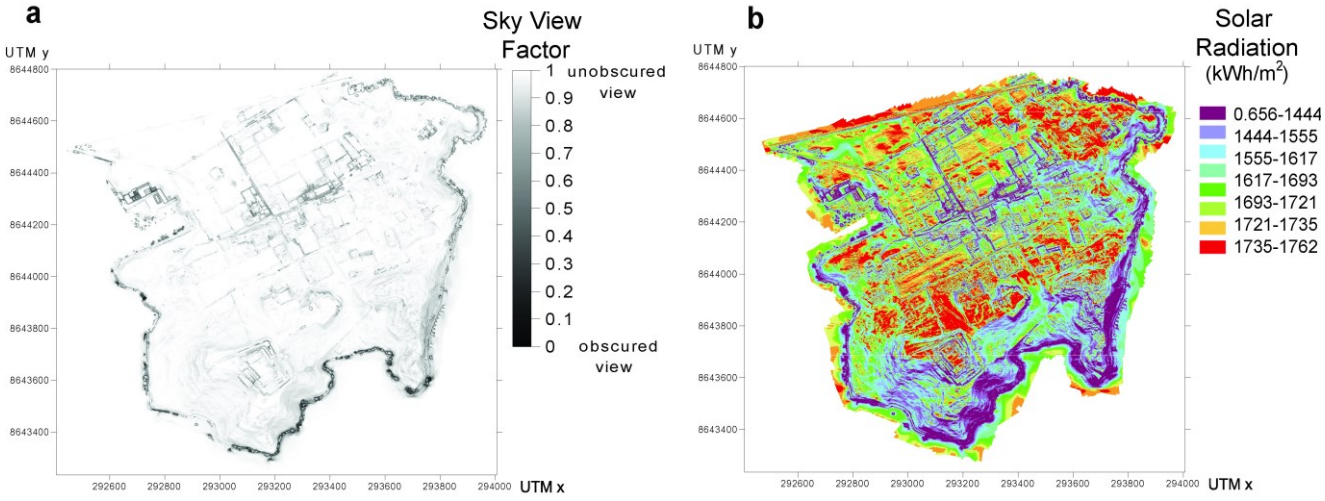

Figure 6. Spatial distribution of the sky view factor (**a**) and annual solar radiation (**b**) at the Sanctuary of Pachacamac.

Subsequently, an OBIA classification is applied to identify the areas most exposed to climatic risks, starting with the best-performing DSM visualizations: TWI, SR, WEI, and Slope are used as starting data for this analysis (Figure 7). OBIA procedures involve an

initial step of segmentation in which layers are divided into image-objects. Specifically, we segment the selected layers with the multiresolution algorithm. In the second step, for each visualization, the numerical threshold value indicative of the site's increased exposure to water, wind and insolation is calculated. The calculation involves every image-object derived from the segmentation of the DSM visualization of the whole SP. For the insolation threshold, we select the highest 10% of the whole range value; for the WEI threshold, we select all values > 1 that indicate areas exposed to wind; and for the water runoff and accumulation, we select a threshold that includes a high degree of TWI. We also consider the slope, which determines the impact of water on the surfaces of the structures.

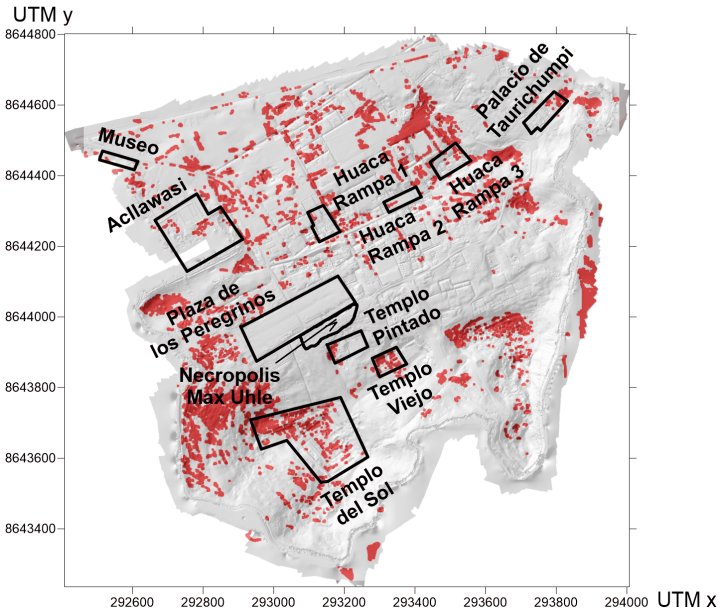

Figure 7. Spatial distribution of the areas of the Sanctuary of Pachacamac exposed to high climatic exposure obtained from OBIA.

4. Results

The results of the morphometric analysis of the DSM are summarized in Figures 3–7. Figure 3a shows the morphological and architectural structure of SP with the flat areas concentrated in the northwestern, northern, and central sectors of SP. These areas mainly consist of the floors of the main constructions (enclosures) and of squares. The higher slopes characterize the southern and eastern sector of SP, where the major hills are located. The TWI map of Figure 3b shows the areas where the rainwater is expected to stagnate or flow (TWI > 3), while the areas with TWI < 3 show peaks and ridges from which the water moves away. The visual inspection of the map in Figure 3b shows that the zones affected by water flow or accumulation are located in the northern sector of the site and along the flanks of the southernmost hill. The central sector of SP also shows areas where the rainwater may accumulate. The relationships among TWI values, slope, and altitude at SP are reported in Figure 3c,d. The inverse relationship between the TWI and slope highlights that the slope plays a major role in controlling the degree of rainwater stagnation or flow at SP. The relationships between TWI and altitude (Figure 3d) are less clear, although the TWI values > 8 concentrate at altitudes less than 30 m above sea level (a.s.l.).

The spatial distribution of the closed depressions, i.e., the areas where the water is expected to stagnate during rain episodes, is reported in Figure 4a. Closed depressions concentrate in the northern and central sector of SP. Because of the prevailing rectangular shape of the depressions, which may be up to 2 m in depth, we deduce that most of them are constituted by the floor of archaeological constructions. Subcircular depressions are

small (less than 5 m in diameter) and show depths < 1 m. These depressions represent archaeological excavations.

The distribution of the total catchment area values (Figure 4b) highlights the areas affected by potential rainwater flows. Diffuse water flow is expected to occur on the slopes of the main hills. Concentrated flows with high TCA values, i.e., streams, may develop not only on the slopes of the hills, but also along (a) the main narrow areas delimited by the perimetral walls of the archaeological constructions and (b) the main and side roads.

The spatial distribution of the WEI values in Figure 5 clearly shows that the areas occupied by the hills located in the southern sector and eastern sector of SP are exposed to winds, whereas the central and the northern sectors are downwind.

Figure 6a shows that the whole SP archaeological site is affected by the sunlight with 95% of the surface having an SVF > 0.7. The map of Figure 6b shows, however, that the altitude plays a major role in the exposure of SP to solar radiation. The higher solar radiation values concentrate on the northern slopes of the hills and on architectural elements such as walls, the floors of constructions delimited by low walls, or open areas (squares).

Figure 7 shows the areas where the impact of solar radiation, wind exposure, surface runoff and stagnation are greatest on the site. Areas with a higher elevation seem to be those most affected by weathering; at the same time, the western side, which faces the coast, also shows a greater propensity to weathering than the other areas of the site.

5. Discussion

The approach used in this study to identify the areas of SP with exposure to climatic factors such as rainfall, winds, and sunlight (solar radiation) differs from those generally implemented for this type of analysis, which are generally scenario-based or probabilistic methods (e.g., [32,33]). These latter methods cannot be reasonably applied to SP because the available meteorological and climatic data on the coastal area of central Peru are sparse, and, when available, have been acquired in very recent times (within the last few years). This prevents the elaboration and application of reliable forecast climatic models and, as a consequence, of scenario-based or probabilistic models of hydrological hazards [31]. In addition, studies on the potential impact of climatic phenomena on a territory usually consider only the terrain morphology and not the spatial structure and geometry of the architectural elements [70–72], although recent studies on modern urban areas show that these elements guide the distribution of flow/stagnation of rainwater [73–75]. The results of our study, which include data on both the terrain morphology and the 3D structure of the SP ceremonial and residential archaeological complex, demonstrate how the exposure to rainwater stagnation or flow, wind, and solar radiation is controlled by the architectural layout. In particular, the results displayed in Figure 3b show that the walls of the SP rectangular enclosures, temples, huacas, and the top of the main hills are sites of drainage divide (watershed), while the rainwater-stagnation and -flow areas concentrate on the floor of the architectural structures and slopes of the main hills, respectively. Among the main constructions of particular archaeological interest depicted in Figure 2, Accllawasi represents the site with the highest exposure to rainwater stagnation (Figure 4a). The zones located northeast of the Plaza de los Peregrinos and in the northern sector of SP are also affected by potential stagnation phenomena. A solution to ensure the security of the pedestrians (both tourists and archaeologists) is to revoke access to these areas during intense rain episodes. This is also applicable for the areas subjected to waterflows shown in Figure 4b, in which the base of the hills and the whole tourist route are identified as potentially dangerous areas, i.e., those with the higher values of TCA. Interestingly, the tourist routes act as channels during rain episodes, with these channels usually being planned to be 20 to 50 cm below the surrounding topography and intended to be laterally confined by the perimetral walls of the constructions. The exposure of the SP site to the wind is mainly controlled by the topography of the upwind areas with WEI > 1.1 concentrated on the top of the main hills. Therefore, the sites of particular interest (shown in Figure 2) with the higher exposure to the wind are Templo del Sol, Templo Viejo, Palacio

de Taurichumpi, and Huacas, with ramp 2 and 3. Templo Pintado is located in an area with moderate exposure to the wind (WEI~1.1). The data from Figure 4b show that the topography is the main controlling factor of the annual solar radiation, and the largest values are concentrated on the northern slopes of the hills, as reported in the Results section. High values of the SR (>1721 kWh/m^2) affect Templo del Sol, Templo Vejo, Templo Pintado, Necropolis Max Uhle, Plaza de los Peregrinos, and Palacio de Taurichumpi. This is because SVF, which is a parameter proportional to the diffuse solar radiation [67], is mostly >0.9 on the whole SP site.

The above-reported conclusions clearly demonstrate that the SP site has elevated exposure to rainfall, winds, and solar radiation. However, while the architectural layout of the SP ceremonial and residential constructions strictly controls the location of the areas potentially affected by the water stagnation or flow due to rainfall, the exposure to winds and solar radiation is mainly controlled by the topography. We conclude that evaluating the exposure to climatic factors of archaeological sites requires additional context in the form of the topography and the 3D structure of the site. Therefore, the use of DSM, with the whole range of surface elements, should be preferred to that of Digital Terrain Models (DTMs), which are limited to a 3D reconstruction of the topography. At the methodological level, even the implementation of expert knowledge-based rules dedicated to the classification and automation of data analysis procedures still offers valuable opportunities, especially when datasets remain limited. In fact, the most recent developments in the field of automatic analysis and artificial intelligence applications in archaeology have been oriented towards Machine Learning techniques; however, these require a massive amount of data [76] that are not available for case studies such as that of SP.

We note that the morphometric analysis proposed in this study could be exported to other archaeological sites for which (a) the available meteorological/climatic data prevent the use of reliable probabilistic and/or scenario-based models or (b) an expeditious analysis is required, e.g., in case of short-term rainfall and/or wind warnings.

6. Conclusions

The results of this study may be summarized in the following main points:

4. DSMs of archaeological sites may be used to define the areas and structures subjected to potential damage from climatic/meteorological events.
5. Object-based image analysis provides a critical tool for evaluating the combined contribution of multiple risk exposures and identifying the areas which are subject to major environmental and climatic threats.
6. The degree to which archaeological sites are exposed to rainwater flow or stagnation, winds, and solar radiation may be obtained based on the combined analysis of DSMs, morphometric parameters, and climatic/meteorological data.
7. The degree of exposure of the SP architectural structures of particular archaeological interest to the above-reported natural phenomena is quantified.
8. The architectural layout of archaeological sites plays a major role in controlling the spatial distribution of the areas subjected to water flow or stagnation, whereas the exposure to winds and solar radiation and winds is manly controlled by the topographic elements as hills and plains.
9. At SP, the tourist routes may act as channels during heavy rain, whereas the walls of the main constructions act as a watershed and delimit the areas where the water may stagnate.

The methodological approach proposed here provides key information relevant to the correct planning of actions intended to preserve our archaeological heritage and could be used at other sites worldwide.

Author Contributions: Conceptualization, L.M. and G.V.; methodology, L.M. and G.V.; software, L.M.; validation, L.M., G.V., R.A. and M.I.P.A.; formal analysis, L.M., G.V. and M.I.P.A.; resources, D.P.-E. and M.I.P.A.; data curation, G.V.; writing—original draft preparation, L.M., D.P.-E., J.O.,

R.A., M.I.P.A. and G.V.; writing—review and editing, L.M., M.I.P.A. and G.V.; visualization, G.V.; supervision, G.V.; project administration, M.I.P.A. and D.P.-E.; funding acquisition, M.I.P.A. All authors have read and agreed to the published version of the manuscript.

Funding: This research has been carried out thanks to the infrastructures and internal funds of the Roma1 and ONT sections of Istituto Nazionale di Geofisica e Vulcanologia, Italy. This study has been carried out within the activities of the project 'Huacas' (Ministero degli Affari Esteri e della Cooperazione Internazionale, Italy) to Maria Ilaria Panaccione Apa.

Data Availability Statement: The data in this article are subject to embargo due to the legal constraints of Ministry of Culture of Peru.

Acknowledgments: We thank Carlo Wester La Torre and the colleagues of INGV, Museum of Pachacamac, Museo Arqueológico Nacional Brüning for the discussions.

Conflicts of Interest: The authors declare no conflicts of interest.

References

1. Kintigh, K.W.; Altschul, J.H.; Beaudry, M.C.; Drennan, R.D.; Kinzig, A.P.; Kohler, T.A.; Limp, W.F.; Maschner, H.D.G.; Michener, W.K.; Pauketat, T.R.; et al. Grand Challenges for Archaeology. *Am. Antiq.* **2014**, *79*, 5–24. https://doi.org/10.7183/0002-7316.79.1.5.
2. Xiao, W.; Mills, J.; Guidi, G.; Rodríguez-Gonzálvez, P.; Gonizzi Barsanti, S.; González-Aguilera, D. Geoinformatics for the Conservation and Promotion of Cultural Heritage in Support of the UN Sustainable Development Goals. *ISPRS J. Photogramm. Remote Sens.* **2018**, *142*, 389–406. https://doi.org/10.1016/j.isprsjprs.2018.01.001.
3. Nations, U. *Transforming Our World: The 2030 Agenda for Sustainable Development*; United Nations, Department of Economic and Social Affairs: New York, NY, USA, 2015.
4. Cunliffe, E. Archaeological Site Damage in the Cycle of War and Peace: A Syrian Case Study. *J. East. Mediterr. Archaeol. Herit. Stud.* **2014**, *2*, 229–247. https://doi.org/10.5325/jeasmedarcherstu.2.3.0229.
5. Darvill, T.; Wainwright, G. The Monuments at Risk Survey: An Introduction. *Antiquity* **1994**, *68*, 820–824. https://doi.org/10.1017/S0003598X00047517.
6. Blaikie, P.; Cannon, T.; Davis, I.; Wisner, B. *At Risk. Natural Hazards, People's Vulnerability and Disasters*; Routledge: London, UK, 2014; ISBN 9781135642723.
7. Ravankhah, M.; de Wit, R.; Argyriou, A.V.; Chliaoutakis, A.; Revez, M.J.; Birkmann, J.; Žuvela-Aloise, M.; Sarris, A.; Tzigounaki, A.; Giapitsoglou, K. Integrated Assessment of Natural Hazards, Including Climate Change's Influences, for Cultural Heritage Sites: The Case of the Historic Centre of Rethymno in Greece. *Int. J. Disaster Risk Sci.* **2019**, *10*, 343–361. https://doi.org/10.1007/s13753-019-00235-z.
8. Smith, K.; Fearnley, C.J.; Dixon, D.; Bird, D.K.; Kelman, I. *Environmental Hazards*; Routledge: London, UK, 2023; ISBN 9781351261647.
9. Contreras, D.A.; Brodie, N. The Utility of Publicly-Available Satellite Imagery for Investigating Looting of Archaeological Sites in Jordan. *J. Field Archaeol.* **2010**, *35*, 101–114. https://doi.org/10.1179/009346910X12707320296838.
10. Evans, D.H.; Fletcher, R.J.; Pottier, C.; Chevance, J.-B.; Soutif, D.; Tan, B.S.; Im, S.; Ea, D.; Tin, T.; Kim, S.; et al. Uncovering Archaeological Landscapes at Angkor Using Lidar. *Proc. Natl. Acad. Sci. USA* **2013**, *110*, 12595–12600. https://doi.org/10.1073/pnas.1306539110.
11. Fisher, C.T.; Cohen, A.S.; Fernández-Diaz, J.C.; Leisz, S.J. The Application of Airborne Mapping LiDAR for the Documentation of Ancient Cities and Regions in Tropical Regions. *Quat. Int.* **2017**, *448*, 129–138. https://doi.org/10.1016/j.quaint.2016.08.050.
12. Kincey, M.; Gerrard, C.; Warburton, J. Quantifying Erosion of 'at Risk' Archaeological Sites Using Repeat Terrestrial Laser Scanning. *J. Archaeol. Sci. Rep.* **2017**, *12*, 405–424. https://doi.org/10.1016/j.jasrep.2017.02.003.
13. Inomata, T.; Triadan, D.; Pinzón, F.; Burham, M.; Ranchos, J.L.; Aoyama, K.; Haraguchi, T. Archaeological Application of Airborne LiDAR to Examine Social Changes in the Ceibal Region of the Maya Lowlands. *PLoS ONE* **2018**, *13*, e0191619. https://doi.org/10.1371/journal.pone.0191619.
14. Risbøl, O.; Gustavsen, L. LiDAR from Drones Employed for Mapping Archaeology—Potential, Benefits and Challenges. *Archaeol. Prospect.* **2018**, *25*, 329–338. https://doi.org/10.1002/arp.1712.
15. Garrison, T.G.; Houston, S.; Alcover Firpi, O. Recentering the Rural: Lidar and Articulated Landscapes among the Maya. *J. Anthropol. Archaeol.* **2019**, *53*, 133–146. https://doi.org/10.1016/j.jaa.2018.11.005.
16. Magnini, L.; Bettineschi, C. Object-Based Predictive Modeling (OBPM) for Archaeology: Finding Control Places in Mountainous Environments. *Remote Sens.* **2021**, *13*, 1197. https://doi.org/10.3390/rs13061197.
17. Bettineschi, C.; Magnini, L.; Azzalin, G.; De Guio, A. Clearence Cairnfields Forever: Combining AI and LiDAR Data in the Marcesina Upland (Northern Italy). *Eur. J. Postclassical Archaeol.* **2022**, *12*, 49–68.
18. Magnini, L.; De Guio, A.; Bettineschi, C. Remote Sensing and Artificial Intelligence for Mountain Archaeology. In *The Oxford Handbook of Mountain Archaeology*; Oxford University Press: Oxford, UK, 2024.

19. Beven, K.J.; Kirkby, M.J. A Physically Based, Variable Contributing Area Model of Basin Hydrology/Un Modèle à Base Physique de Zone d'appel Variable de l'hydrologie Du Bassin Versant. *Hydrol. Sci. Bull.* **1979**, *24*, 43–69. https://doi.org/10.1080/02626667909491834.
20. Marsh, A.; Fleitmann, D.; Al-Manmi, D.A.M.; Altaweel, M.; Wengrow, D.; Carter, R. Mid- to Late-Holocene Archaeology, Environment and Climate in the Northeast Kurdistan Region of Iraq. *Holocene* **2018**, *28*, 955–967. https://doi.org/10.1177/0959683617752843.
21. Agapiou, A.; Lysandrou, V.; Hadjimitsis, D.G. A European-Scale Investigation of Soil Erosion Threat to Subsurface Archaeological Remains. *Remote Sens.* **2020**, *12*, 675. https://doi.org/10.3390/rs12040675.
22. Guiney, R.; Santucci, E.; Valman, S.; Booth, A.; Birley, A.; Haynes, I.; Marsh, S.; Mills, J. Integration and Analysis of Multi-Modal Geospatial Secondary Data to Inform Management of at-Risk Archaeological Sites. *ISPRS Int. J. Geo-Inf.* **2021**, *10*, 575. https://doi.org/10.3390/ijgi10090575.
23. Papageorgiou, N.; Hadjimitsis, D.G. Evaluation of Soil Loss by Water in Archaeological Landscapes by Using the (R)USLE Model and GIS. The Case Study of Paphos District, Cyprus. In *Digital Heritage. Progress in Cultural Heritage: Documentation, Preservation, and Protection: 8th International Conference, EuroMed 2020, Virtual Event, November 2–5, 2020, Revised Selected Papers 8*; Springer: Berlin/Heidelberg, Germany, 2021; pp. 64–77.
24. Forti, L.; Brandolini, F.; Oselini, V.; Peyronel, L.; Pezzotta, A.; Vacca, A.; Zerboni, A. Geomorphological Assessment of the Preservation of Archaeological Tell Sites. *Sci. Rep.* **2023**, *13*, 7683. https://doi.org/10.1038/s41598-023-34490-4.
25. Apa, M.I.P.; La Torre, C.E.W.; Cachay, R.F.G.; Magnini, L.; Murga, J.C.; Ranera, F.; Ventura, G. Quantitative Estimate of the Damages from Human Activities at the Apurlec Monumental Archaeological Complex (7th–14th Century AD, Peru) from Multitemporal Photogrammetry. *Archaeol. Anthropol. Sci.* **2023**, *15*, 110. https://doi.org/10.1007/s12520-023-01818-0.
26. Sandweiss, D.H.; Maasch, K.A.; Burger, R.L.; Richardson, J.B.; Rollins, H.B.; Clement, A. Variation in Holocene El Niño Frequencies: Climate Records and Cultural Consequences in Ancient Peru. *Geology* **2001**, *29*, 603. https://doi.org/10.1130/0091-7613(2001)029<0603:VIHENO>2.0.CO;2.
27. Delle Rose, M. Landscape Modifications Ascribed to El Niño Events in Late Pre-Hispanic Coastal Peru. *Land* **2022**, *11*, 2207. https://doi.org/10.3390/land11122207.
28. Franco, R.; Paredes, P. El Templo Viejo de Pachacamac: Nuevos Aportes Al Estudio Del Horizonte Medio. *Boletín Arqueol. PUCP* **2000**, *4*, 607–630. https://doi.org/10.18800/boletindearqueologiapucp.200001.022.
29. Winsborough, B.M.; Shimada, I.; Newsom, L.A.; Jones, J.G.; Segura, R.A. Paleoenvironmental Catastrophies on the Peruvian Coast Revealed in Lagoon Sediment Cores from Pachacamac. *J. Archaeol. Sci.* **2012**, *39*, 602–614. https://doi.org/10.1016/j.jas.2011.10.018.
30. Vieira, M.T.; Vieira, A.V.; García, C.M.V. Vulnerability Index Elaboration for Climate Change Adaptation in Peru. *Eur. J. Sustain. Dev.* **2019**, *8*, 102. https://doi.org/10.14207/ejsd.2019.v8n5p102.
31. L'Heureux, M.L.; Tippett, M.K.; Takahashi, K.; Barnston, A.G.; Becker, E.J.; Bell, G.D.; Di Liberto, T.E.; Gottschalck, J.; Halpert, M.S.; Hu, Z.-Z.; et al. Strength Outlooks for the El Niño–Southern Oscillation. *Weather Forecast.* **2019**, *34*, 165–175. https://doi.org/10.1175/WAF-D-18-0126.1.
32. Zschau, J. Where Are We with Multihazards, Multirisks Assessment Capacities? In *Science for Disaster Risk Management 2017: Knowing Better and Losing Less*; Poljanšek, K., Marín Ferrer, M., De Groeve, T., Clark, I., Eds.; European Commission: Luxembourg, 2017; pp. 96–128.
33. Appiotti, F.; Assumma, V.; Bottero, M.; Campostrini, P.; Datola, G.; Lombardi, P.; Rinaldi, E. Definition of a Risk Assessment Model within a European Interoperable Database Platform (EID) for Cultural Heritage. *J. Cult. Herit.* **2020**, *46*, 268–277. https://doi.org/10.1016/j.culher.2020.08.001.
34. Davis, D.S. Object-based Image Analysis: A Review of Developments and Future Directions of Automated Feature Detection in Landscape Archaeology. *Archaeol. Prospect*. **2019**, *26*, 155–163. https://doi.org/10.1002/arp.1730.
35. Blaschke, T. Object Based Image Analysis for Remote Sensing. *ISPRS J. Photogramm. Remote Sens.* **2010**, *65*, 2–16. https://doi.org/10.1016/j.isprsjprs.2009.06.004.
36. Magnini, L.; Bettineschi, C. Theory and Practice for an Object-Based Approach in Archaeological Remote Sensing. *J. Archaeol. Sci.* **2019**, *107*, 10–22. https://doi.org/10.1016/j.jas.2019.04.005.
37. Perales Munguía, M.F.; Capriata Estrada, C.; Hidalgo Villanueva, J.P. *Historia y Uso Del Camino Entre Xauxa y Pachacamac: Investigaciones Arqueológicas e Históricas*; Ministerio de Cultura del Peru: Lima, Peru, 2019.
38. Cieza de Leon, P. de Crónica Del Perú. Segunda Parte. *Edición de Francesca Cantú*; Fondo Editorial de la Pontificia Universidad Catolica del Perù—Academia Nacional de la Historia: Lima, Peru.
39. Hyslop, J. *Qhapaqñan. El Sistema Vial Inkaico*; Mujica Barreda, E., Ed.; Instituto Andino de Estudios Arqueológicos (INDEA)—Petróleos del Perú: Lima, Peru, 1992; p. 119p.
40. Estete, M. de Noticia Del Perú (Vol. I). In *El Peru a Traves de Los Siglos*; Editores Tecnicos Asociados Lima: Lima, Peru; pp. 345–402.
41. Millones Santa Gadea, L. La Mirada de Los Conquistadores. In *Pachacamac: El Oráculo en el Horizonte Marino del Sol Poniente*; Banco de Crédito del Perù: Lima, Peru, 2017; pp. 34–47, ISBN 978-9972-837-30-2.
42. Pozzi-Escot, D. *Pachacamac: El Oráculo en el Horizonte Marino del Sol Poniente*; Banco de Crédito del Perù: Lima, Peru, 2017.

43. Makowski, K. Pachacamac y La Política Imperial Inca. In *El Inca y la Huaca. La Religión del Poder y el Poder de la Religión en el Mundo Antiguo*; Curatola, M., Szemiński, J., Eds.; The Hebrew University of Jerusalem y Fondo Editorial PUCP: Lima, Peru, 2016; pp. 153–208.
44. Jiménez, C. *Proyecto de Investigación y Conservación Del Templo Del Sol—Pachacamac*; Lima, Peru, 2011.
45. Franco Jordán, R.G.; Paredes Botoni, P.F. *Templo Viejo de Pachacamac. Dioses, Arquitectura, Sacrificios y Ofrendas*; Institute of Andean Research-Fundación Wiesse: Lima, Peru, 2016; ISBN 9789972293795.
46. Uhle, M. *Pachacamac. Report of the William Pepper M.D., LL.D. Peruvian Expedition of 1896*; University of Pennsylvania Press: Philadelphia, PA, USA, 1903.
47. Ángeles; Rommel; Pozzi-Escot, D. El Horizonte Medio En Pachacamac. In *Arqueología en el Perú. Nuevos Aportes para el Estudio de las Sociedades Andinas Prehispánicas*; Romero, R., Pavel Svendsen, T., Eds.; Anheb Impresiones: Lima, Peru, 2010; pp. 175–196.
48. Eeckhout, P. El Oráculo de Pachacamac y Los Peregrinajes a Larga Escala En Los Andes Prehispánicos. In *Adivinación y Oráculos en las Américas*; Curatola, M., Ziołkowsi, M., Eds.; Lima, Peru, 2008; pp. 161–180.
49. Rostworowski, M. *Pachacamac y El Señor de Los Milagros. Una Trayectoria Milenaria*; Instituto de Estudios Peruanos: Lima, Peru, 1992.
50. Tello, J.C. Pachacamac. *Chaski* **1940**, *1*, 1–4.
51. Tello, J.C. Memoria Sucinta Sobre Los Trabajos Arqueológicos Realizados En Las Ruinas de Pachacámac Durante Los Años 1940 y 1941; Lima, Peru, 1943.
52. Jacay, J.; Oshiro, J. Estudio Geológico de La Laguna Urpiwachaq. In *Urpiwachaq: Gestión y Puesta en Valor de la Laguna*; Pozzi-Escot, D., Oshiro, J., Eds.; Ministerio de Cultura del Perú y Universidad del Pacifico: Lima, Peru, 2015; pp. 21–37.
53. Pozzi-Escot, D.; Oshiro, J.; Romano, G.; Capozzoli, L.; Lasaponara, R.; Masini, N. Traces in the Desert: Use of New Technologies for the Study and Valorization of the Pachacamac Sanctuary—Lima, Peru. *Herit. Sci.* **2018**, *6*, 68. https://doi.org/10.1186/s40494-018-0230-1.
54. Shimada, I.; Segura, R.; Rostworowski; María Hirokatsu, W. Las Prospecciones y Excavaciones En Urpi Kocha y Urpi Wachaq: Estudio Preliminar. In *Cuadernos de Investigación del Archivo Tello N°5. Arqueología de Pachacamac: Excavaciones en Urpi Kocha y Urpi Wachac, Editado por R. Vega-Centeno*; Museo de Arqueología y Antropología y Universidad Nacional Mayor de San Marcos: Lima, Peru, 2007; pp. 13–18.
55. Rostworowski, M. *Recursos Naturales y Pesca, Siglos XVI-XVII/Curacas y Sucesiones, Costa Norte. Obras Completas IV*; IEP: Lima, Peru, 2005.
56. Cappai, M.; Delogu, F.; Pozzi-Escot, D.; Pacheco Neyra, G.; Meloni, P.; Pia, G. Degradation Phenomena of Templo Pintado Painted Plasters. *Constr. Build. Mater.* **2023**, *392*, 131839. https://doi.org/10.1016/j.conbuildmat.2023.131839.
57. Chipana, H.; Abad, J.; Pozzi-Escot, D. *Pachacamac: Levantamiento Arquitectónico Con Drone Del Santuario Arqueológico*; Ministerio; Lima, Peru, 2020.
58. Lagos, P.; Silva, Y.; Nickl, E.; Mosquera, K. El Niño—Related Precipitation Variability in Perú. *Adv. Geosci.* **2008**, *14*, 231–237. https://doi.org/10.5194/adgeo-14-231-2008.
59. Goubanova, K.; Echevin, V.; Dewitte, B.; Codron, F.; Takahashi, K.; Terray, P.; Vrac, M. Statistical Downscaling of Sea-Surface Wind over the Peru–Chile Upwelling Region: Diagnosing the Impact of Climate Change from the IPSL-CM4 Model. *Clim. Dyn.* **2011**, *36*, 1365–1378. https://doi.org/10.1007/s00382-010-0824-0.
60. Kottek, M.; Grieser, J.; Beck, C.; Rudolf, B.; Rubel, F. World Map of the Köppen-Geiger Climate Classification Updated. *Meteorol. Zeitschrift* **2006**, *15*, 259–263. https://doi.org/10.1127/0941-2948/2006/0130.
61. Kopecký, M.; Macek, M.; Wild, J. Topographic Wetness Index Calculation Guidelines Based on Measured Soil Moisture and Plant Species Composition. *Sci. Total Environ.* **2020**, *757*, 143785. https://doi.org/10.1016/j.scitotenv.2020.143785.
62. Pardo-Igúzquiza, E.; Dowd, P.A. The Mapping of Closed Depressions and Its Contribution to the Geodiversity Inventory. *Int. J. Geoheritage Park.* **2021**, *9*, 480–495. https://doi.org/10.1016/j.ijgeop.2021.11.007.
63. Wang, L.; Liu, H. An Efficient Method for Identifying and Filling Surface Depressions in Digital Elevation Models for Hydrologic Analysis and Modelling. *Int. J. Geogr. Inf. Sci.* **2006**, *20*, 193–213. https://doi.org/10.1080/13658810500433453.
64. Quinn, P.; Beven, K.; Chevallier, P.; Planchon, O. The Prediction of Hillslope Flow Paths for Distributed Hydrological Modelling Using Digital Terrain Models. *Hydrol. Process.* **1991**, *5*, 59–79. https://doi.org/10.1002/hyp.3360050106.
65. Conrad, O.; Bechtel, B.; Bock, M.; Dietrich, H.; Fischer, E.; Gerlitz, L.; Wehberg, J.; Wichmann, V.; Böhner, J. System for Automated Geoscientific Analyses (SAGA) v. 2.1.4. *Geosci. Model Dev.* **2015**, *8*, 1991–2007. https://doi.org/10.5194/gmd-8-1991-2015.
66. Böhner, J.; Antonić, O. Chapter 8 Land-Surface Parameters Specific to Topo-Climatology. In *Developments in Soil Science*; Elsevier: Amsterdam, The Netherlands, 2009; pp. 195–226.
67. Zakšek, K.; Oštir, K.; Kokalj, Ž. Sky-View Factor as a Relief Visualization Technique. *Remote Sens.* **2011**, *3*, 398–415. https://doi.org/10.3390/rs3020398.
68. Fu, P.; Rich, P.M. Design and Implementation of the Solar Analyst: An ArcView Extension for Modeling Solar Radiation at Landscape Scales. In Proceedings of the Nineteenth Annual ESRI User Conference, San Diego, CA, USA, 26–30 July 1999; pp. 1–31.
69. Kidd, C.; Chapman, L. Derivation of Sky-View Factors from Lidar Data. *Int. J. Remote Sens.* **2012**, *33*, 3640–3652. https://doi.org/10.1080/01431161.2011.635163.
70. Blocken, B.; Carmeliet, J. A Review of Wind-Driven Rain Research in Building Science. *J. Wind Eng. Ind. Aerodyn.* **2004**, *92*, 1079–1130. https://doi.org/10.1016/j.jweia.2004.06.003.

71. Brimblecombe, P.; Grossi, C.M. Damage to Buildings from Future Climate and Pollution. *APT Bull. J. Preserv. Technol.* **2007**, *38*, 13–18.
72. Sesana, E.; Gagnon, A.S.; Ciantelli, C.; Cassar, J.; Hughes, J.J. Climate Change Impacts on Cultural Heritage: A Literature Review. *WIREs Clim. Chang.* **2021**, *12*, e710. https://doi.org/10.1002/wcc.710.
73. Park, K.; Won, J. Analysis on Distribution Characteristics of Building Use with Risk Zone Classification Based on Urban Flood Risk Assessment. *Int. J. Disaster Risk Reduct.* **2019**, *38*, 101192. https://doi.org/10.1016/j.ijdrr.2019.101192.
74. Azizi, K.; Diko, S.K.; Saija, L.; Zamani, M.G.; Meier, C.I. Integrated Community-Based Approaches to Urban Pluvial Flooding Research, Trends and Future Directions: A Review. *Urban Clim.* **2022**, *44*, 101237. https://doi.org/10.1016/j.uclim.2022.101237.
75. Zhu, Z.; Gou, L.; Liu, S.; Peng, D. Effect of Urban Neighbourhood Layout on the Flood Intrusion Rate of Residential Buildings and Associated Risk for Pedestrians. *Sustain. Cities Soc.* **2023**, *92*, 104485. https://doi.org/10.1016/j.scs.2023.104485.
76. Argyrou, A.; Agapiou, A. A Review of Artificial Intelligence and Remote Sensing for Archaeo-logical Research. *Remote Sens.* **2022**, *14*, 6000. https://doi.org/10.3390/rs14236000.